A Bond−Bond Description of the Intermolecular Interaction Energy: The Case of the Weakly Bound Acetylene−Hydrogen Complex†

F. Thibault,*,‡ D. Cappelletti,§ F. Pirani,|| and M. Bartolomei⊥

Institut de Physique de Rennes, UMR CNRS 6251, Université de Rennes I, F-35042 Rennes, France, Dipartimento di Ingegneria Civile ed Ambientale Universita di Perugia, 06100 Perugia, Italy, Dipartimento di Chimica, Universita di Perugia, 06100 Perugia, Italy, and Instituto de Física Fundamental, CSIC, Serrano 123, 28006 Madrid, Spain

Received: May 29, 2009; Revised Manuscript Received: September 28, 2009

A new semiempirical potential energy surface (PES) for the acetylene−hydrogen system has been derived by using the recently introduced bond−bond methodology. The proposed PES, expressed in an analytic form suitable for molecular dynamics simulations, involves a limited number of parameters, each one having a physical meaning and allowing the accurate description of the system also in the less stable configurations. The analysis of novel integral cross sections data, measured with nearly effusive molecular beams, combined with that of available pressure broadening coefficients of isotropic Raman lines at 143 K and IR lines at 173 and 295 K of C_2H_2 in H_2, provides a test of the reliability of the proposed PES and suggests also some refinements. An extensive comparison with a recent ab initio potential is also exploited.

I. Introduction

Gaseous mixtures of acetylene and hydrogen molecules are relevant for many fundamental and applied issues. Both species contribute to the atmospheric composition of the giant planets of the solar system and also to their atmospheric photochemistry.[1] Applications include combustion research[2,3] and flame diagnostics,[4] diamond-like chemical vapor deposition,[5] and PAH[6] and carbon nanotube growth.[7]

Indeed, all the collisional and optical properties of the acetylene−hydrogen interaction aggregates are determined by the intermolecular potential energy surface (PES). Ethyne is the simplest hydrocarbon with a triple carbon−carbon bond which makes it a sort of prototype apolar and strongly anisotropic molecule with peculiar intermolecular interaction. Hydrogen being the simplest molecule is amenable of very accurate quantum chemical calculations.

In this work we combine results from semiempirical methods, ab initio calculations, molecular beam scattering experiments, and pressure broadening coefficient investigations in order to better understand the nature of intermolecular forces in the $C_2H_2-H_2$ system and to apply and extend simple and physically grounded analytical functions for their representation. This has been a general subject in physical chemistry along the years.[8−10] In this paper we complete a series of studies of the acetylene gas phase complexes, which already includes C_2H_2-Ar[11] C_2H_2-Kr, and C_2H_2-Xe[12] C_2H_2-Ne.[13]

This effort is currently motivated in particular by the aim of generating better force fields for model simulations of molecular aggregates, both in the gas phase and in the condensed matter conditions of interest in several applications, particularly in astrophysics.[14] With this respect, the speed of computation of the force field is a primary need which can influence the size (and the accuracy) of the largest simulations, even with modern computers. This is the reason why the venerable Lennard-Jones potential model, with all its limitations, is still by far the most used intermolecular functional form in molecular dynamics studies.

An additional challenging problem concerns the detailed representation of the PES, especially when arising from noncovalent interaction components, which often includes exchange repulsion (in the following also called size repulsion) at short range and electrostatic, induction, and dispersion contributions at long range. Usually, the van der Waals (vdW) component of the interaction, which we assume here to be determined by the combination of size repulsion with dispersion attraction (even if alternative definitions can be found in literature) is the most difficult to be characterized. Representation and modeling of vdW in atom−atom, ion−atom (vdW plus induction), and atom−simple molecule systems have been often achieved by using semiempirical[15−18] and empirical[19−22] methods.

Very recently[23] some of the authors have introduced a new semiempirical methodology to easily and efficiently represent the full PES in weakly bound systems as a combination of few effective terms representative of the leading interaction components. Such terms have been defined by simple formulas involving a few parameters with a definite physical meaning, typically related to basic physical properties of the interacting partners as the atomic and molecular bond polarizabilities and permanent multipole moments. In particular, diatom−diatom complexes have been accurately described[23,24] by representing vdW as a single bond−bond pair contribution. Herein, we extend the methodology to a more complex system involving a polyatomic partner as C_2H_2. New scattering experiments have been performed and the measured integral cross section (ICS) data have been used, together with pressure broadening (PB) coefficients, to test and to improve the reliability of the proposed PES. Extensive comparisons with ab initio calculations of the intermolecular interaction have been also exploited.

Section II presents the new formulation of the PES and summarizes the main features of ab initio calculations. Section

† Part of the "Vincenzo Aquilanti Festschrift".
* Corresponding author.
‡ IPR Rennes I.
§ DICA, Universita di Perugia.
|| Dipartimento di Chimica, Universita di Perugia.
⊥ CSIC Madrid.

10.1021/jp905055n
Published on Web 10/20/2009

III describes the scattering experiments and their analysis carried out calculating simultaneously PB coefficients (section IV). The optimization of the PES parameters and the comparison with experimental results is presented in section V. Summary and conclusions follow in section VI.

II. Bond−Bond Representation of the PES

The intermolecular energy V is represented here as combination of two effective interaction components

$$V = V_{\mathrm{vdW}} + V_{\mathrm{elect}} \tag{1}$$

In (1) V_{vdW} is the van der Waals interaction and V_{elect} accounts for the electrostatic interaction, arising from anisotropic molecular charge distributions, that here asymptotically must provide the permanent quadrupole−permanent quadrupole term. Both interaction components depend on R, the distance between the centers of mass of acetylene and hydrogen, and on Θ_a, Θ_b, Φ, the Jacobi angular coordinates which describe the relative orientation of the two molecules.

The total van der Waals term, V_{vdW}, is given as a sum of the contributions corresponding to the different $\mathrm{bond_a}-\mathrm{bond_b}$ i pairs, counted considering all the bonds located on the two monomers a and b (C_2H_2 is the a monomer)

$$V_{\mathrm{vdW}}(R, \Theta_a, \Theta_b, \Phi) = \sum_i V^i_{\mathrm{vdW}} \tag{2}$$

This representation of V_{vdW} exploits the additivity of bond polarizability components in determining the full molecular polarizability (the basic property controlling vdW). Moreover, since each bond polarizability component is different from the sum of the free atom contributions, the proposed methodology indirectly accounts for three body effects.[25]

For the present system we have three bond−bond contributions corresponding to two CH−HH and one CC−HH pairs.

The analytical representation of each bond−bond contribution, V^i_{vdW}, is an extension and generalization of the atom-bond pairwise additivity concept.[25,26] In particular V^i_{vdW} must depend on the distance R_i between the bond midpoints, and θ_{ai}, θ_{bi}, ϕ_i, the four body Jacobi angular coordinates which describe the relative orientation of the two bonds. It is important to note that each of the bonds considered is here assumed to be an independent diatomic subunit having electronic charge distribution of nearly cylindrical symmetry and that the reference point for each bond is set to coincide with the geometric bond center since the dispersion center and the bond center coincide for CC and HH and are almost coincident for CH.[25,26]

The parametrization adopted for each V^i_{vdW} is of the Improved Lennard-Jones (ILJ) type[27]

$$\frac{V^i_{\mathrm{vdW}}(R_i, \gamma_i)}{\varepsilon_i(\gamma_i)} = f(x_i) = \left[\frac{6}{n(x_i) - 6}\left(\frac{1}{x_i}\right)^{n(x_i)} - \frac{n(x_i)}{n(x_i) - 6}\left(\frac{1}{x_i}\right)^6\right] \tag{3}$$

where x_i is a reduced distance

$$x_i = \frac{R_i}{R_{mi}(\gamma_i)} \tag{4}$$

In eq 3, for compactness each $\gamma_i = (\theta_{ai}, \theta_{bi}, \phi_i)$ and ε_i and R_{mi} are the interaction well depth (the i bond−bond pair binding energy) and its location, respectively. We note that the ILJ function[27] is much more flexible than its classic Lennard-Jones(12,6) precursor and gives a more realistic representation of both the size repulsion (first term in square brackets) and the long-range dispersion attraction (second term in square brackets).

The n term is expressed as a function of both R_i and γ_i using the following empirical equation[26]

$$n(x_i) = \beta + 4.0x_i^2 \tag{5}$$

β is a parameter which depends on the nature and hardness of interacting particles. For the present systems β has been fixed to 9 for both CH−HH and CC−HH bond−bond couples.

The angle dependence of V^i_{vdW} is obtained by representing the potential parameters ε_i and R_{mi} in a spherical harmonic expansion. In this way $f(x_i)$, the reduced form of the bond−bond potentials (see ref 26), is taken to be the same for all orientations, as also stressed in previous work.[28−31] If necessary, for cases more complex than the present system the β parameter can be allowed to vary with the angles γ_i, making more flexible the shape of the PES. Moreover, it should be stressed that introducing the angular dependence as an expansion of the potential parameters provides a much faster convergence on V^i_{vdW} than by directly expanding it in terms of radial coefficients.[23,24,32] For the purpose of the present work we find it sufficient to truncate the expansion to the fifth term

$$\varepsilon_i(\gamma) = \varepsilon_i^{000} + \varepsilon_i^{202}A^{202}(\gamma) + \varepsilon_i^{022}A^{022}(\gamma) + \varepsilon_i^{220}A^{220}(\gamma) + \varepsilon_i^{222}A^{222}(\gamma) \tag{6}$$

$$R_{mi}(\gamma) = R_{mi}^{000} + R_{mi}^{202}A^{202}(\gamma) + R_{mi}^{022}A^{022}(\gamma) + R_{mi}^{220}A^{220}(\gamma) + R_{mi}^{222}A^{222}(\gamma) \tag{7}$$

where the $A^{L_1L_2L}(\gamma)$ are bipolar spherical harmonics.[33]

In Appendix A of ref 23, a method to estimate the ε_i and R_{mi} potential parameters from diatomic (or molecular bond) polarizability values has been reported. Specifically, this has been done for five relevant configurations of each i bond−bond pair, specifically $H(\theta_{ai} = 90°, \theta_{bi} = 90°, \phi_i = 0°)$, $X(90,90,90)$, T_a $(90,0,0)$, T_b $(0,90,0)$, $L(0,0,0)$.[34] The method provides the same parameters for the X and H geometries. Once ε_i and R_{mi} for the five selected geometries are known, they allow the preangular coefficients $\varepsilon_i^{L_1L_2L}$ and $R_{mi}^{L_1L_2L}$ to be obtained by a simple inversion of eqs 6 and 7.[23] The latter allow a first-order full PES to be generated and the ε_i and R_{mi} parameters can be refined during the fitting of the experimental data.

For the V_{elect} component (second term of eq 1), the usual approximated expression depending on the product of molecular quadrupoles Q (see eq 9 of ref 23) is not sufficiently accurate for the present purposes because the separation among the molecular charges on acetylene is not negligible with respect to the probed intermolecular distances.[9] Therefore, we assumed two molecular charge distributions, on acetylene and hydrogen, compatible with the respective molecular quadrupoles, and adopted the following sum of Coulomb potentials

$$V_{\text{elect}}(R, \Theta_a, \Theta_b, \Phi) = \sum_{jk} \frac{q_{ja} q_{kb}}{r_{jk}} \quad (8)$$

where q_{ja} and q_{kb} are point charges located on monomers a and b, respectively, and r_{jk} is the distance between them. This representation should be used for cases where the molecular dimensions are not negligible with respect to the intermolecular distance R.[9] For both monomers a linear distribution of charges along the main axis has been chosen: $r_{\pm}$ defines the position of the point charge $q_{\pm}$ along the molecular axis and represents the distance with respect to the molecular center of mass (CM) (note that for both monomers $q_{-} = -2\ q_{+}$ and that two positive charges are placed symmetrically with respect to the molecular CM). The parameters determining the charge distributions have been slightly adjusted, during the analysis of the experimental data and taking into account also ab initio calculations (see below), in order to reproduce within few percent the molecular quadrupoles.

All the parameters of the $C_2H_2-H_2$ PES are given in Table 1 and the main features of the intermolecular energy V in five selected geometries of the interacting system are reported in Table 2 and Figure 1.

Recently[35] extensive ab initio calculations of the intermolecular potential of the $C_2H_2-H_2$ system have been performed at the CCSD(T) (coupled cluster including single and double and noniterative triple excitations) and at the SAPT(DFT) levels of theory. A global representation (four dimensions) of the PES was given and whose accuracy was tested on pressure broadening coefficients measurements.[35] These ab initio results are used in the present paper as an important check of the bond−bond methodology.

To this aim, some relevant cuts of this ab initio PES are plotted in Figure 1. The corresponding equilibrium distances and binding energies are also reported in Table 2. The comparison between the ab initio and the optimized bond−bond PESs (see Figure 1 and Table 2) indicates that the sequence of the selected configurations, the absolute energies, and the overall anisotropy are globally in a good agreement.

In more detail we note that in the case of the ab initio PES, the position of the potential wells is slightly shifted at larger intermolecular distances for the H, X, and L configurations of the molecule−molecule aggregate, while the opposite can be seen for the T_a, T_b, and S_{45} ($\Theta_a = 45°$, $\Theta_b = 45°$, $\Phi = 0°$) geometries.

An alternative comparison between the present and the ab initio PESs is shown in Figure 2 where the isotropic ($V^{000}(R)$) and anisotropic components are plotted. To this aim, the latter have been obtained by expanding each PES in bipolar spherical harmonics. Since the method is identical to that used in ref 35 (eq 2), it is not described here. An inspection of Figure 2 suggests again that the two PESs are quite similar and that the quadrupole−quadrupole interaction, which is the main contribution[35] to the V^{224} term at long range, is well estimated by the bond−bond representation. Moreover, the spherically averaged interaction of the ab initio PES is slightly deeper and located at a slightly lower distance. The lower panels of Figure 2 show that the bond−bond PES is more anisotropic at short range while the ab initio PES is slightly more anisotropic for $R > 4.2$ Å. These differences will affect the agreement with the experimental data as described in the following.

III. Integral Cross Section Measurements and Calculations

The basic structure of the experimental apparatus for integral cross section measurements has been already described previously,[33,36] so that we will report here in detail only the modifications introduced for the present investigation. Briefly, the setup consists of a sequence of differentially pumped vacuum chambers, where a molecular beam (MB) is produced, collimated by a set of defining slits, velocity selected and attenuated by collisions with a gaseous target. The velocity selector is a mechanical device made up by six rotating slotted disks[37] allowing the selection of molecules with a velocity v and fwhm (full width at half-maximum) better than 5%. The MB intensity is monitored by a quadrupole mass spectrometer, in line of sight with the MB source. The total (elastic + inelastic) integral cross section Q is obtained, at a given selected MB velocity v, measuring the MB intensity attenuation due to the target gas presence in the scattering box. The calibration of the absolute scale of $Q(v)$ is obtained following the procedure illustrated in refs 38 and 39.

In the present experiment we employed D_2 as projectile and kept C_2H_2 in the scattering chamber, maintained at 90 K. This choice allows us to achieve the best kinematic resolution conditions and the highest possible signal-to-noise ratio. For the present experiment a MB source has been used which can

TABLE 1: Optimized R_{mi} (Å) and ε_i (meV) Parameters and (in parentheses) Predicted Values Estimated at the Equilibrium Bond Length r_{eq} (Å) and Considering the Spherical $\bar{\alpha}$ and Anisotropic $\Delta\alpha$ Bond Polarizability Values (Å^3)[d]

bond−bond		R_{mi}	ε_i
C−C−H_2	H = X	3.84 (3.69)	3.31 (4.19)
	T_a	3.90 (3.82)	3.77 (4.24)
	T_b	3.93 (4.07)	4.74 (3.86)
	L	4.04 (4.18)	4.65 (3.78)
	β	9	
C−H−H_2	H = X	3.58 (3.44)	2.39 (3.02)
	T_a	3.67 (3.60)	2.50 (2.82)
	T_b	3.41 (3.53)	4.13 (3.36)
	L	3.56 (3.69)	3.76 (3.06)
	β	9	

bond	r_{eq}	$\bar{\alpha}$[a]	$\Delta\alpha$[a]
H_2	0.7668[b]	0.789	0.299
C−C	1.203[c]	1.774	1.794
C−H	1.068[c]	0.701	0.358

monomer	Q	q_{-} (r_{-})	q_{+} (r_{+})
H_2	0.4824	−0.9190 (0.0)	0.4595 (±0.3834)
C_2H_2	4.35	−0.6088 (0.0)	0.3044 (±1.4145)

[a] From ref 23. [b] From ref 54. [c] From ref 55. [d] Quadrupole moments Q and point charges $q_{\pm}$ are in a.u. The $r_{\pm}$ distances are in angstroms.

TABLE 2: Binding Energy D_e (meV) and Equilibrium Intermolecular Distance R_e (Å) Associated to the Spherically Averaged Total Interaction $\bar{V}$ and to the Intermolecular Potentials V in the Relevant Geometries of the $C_2H_2-H_2$ Complex, As Obtained with the Present Method and Ab Initio Calculations[35]

	bond−bond		ab initio	
	R_e	D_e	R_e	D_e
$\bar{V}$	4.17	6.08	4.09	6.45
V^H	3.92	2.22	4.00	1.98
V^X	3.76	5.27	3.83	4.34
V^{T_a}	3.58	16.54	3.52	17.50
V^{T_b}	4.33	13.31	4.26	15.16
V^L	5.13	−0.33	5.14	−1.00
$V^{S_{45}}$	4.01	12.32	3.87	14.36

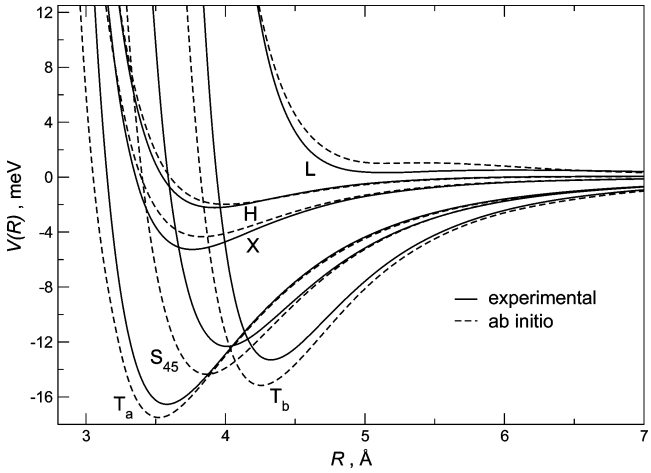

Figure 1. Comparison between ab initio and bond−bond PESs for selected configurations of the $C_2H_2-H_2$ system.

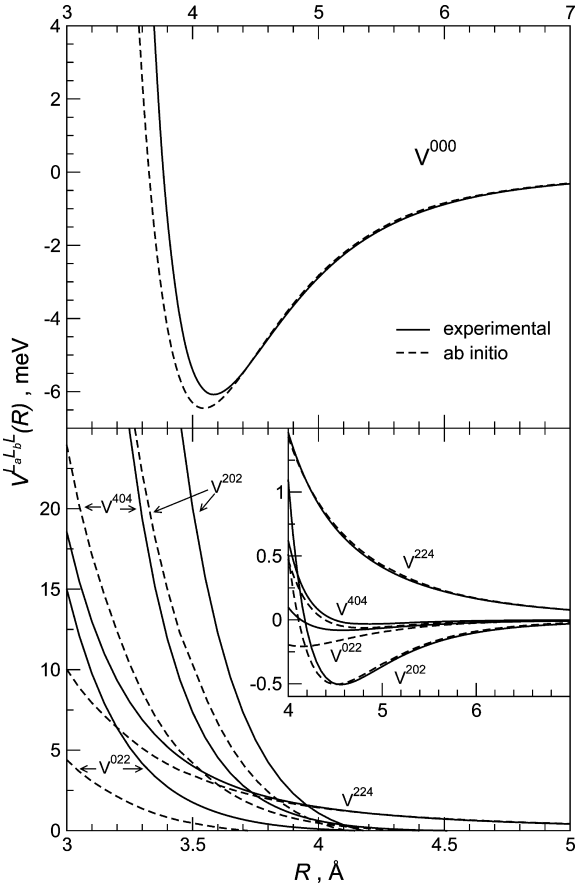

Figure 2. Comparison, for the present bond−bond PES (solid line) and the ab initio PES[35] (dashed line), between the spherically averaged total interactions (top) and main anisotropic (bottom) components. Note that, as compared to Figure 2 of ref 35, these components are here rescaled by a factor $(4\pi)^{3/2}$ to enhance the differences at short range.

operate both at room temperature and also at 90 K, by adding a liquid nitrogen system able to cool the nozzle. This has been necessary to extend the velocity range of the D_2 MB in order to observe two extrema of the quantum *glory* oscillation.

Experimental results are shown in Figure 3, where $Q(v)$ is plotted multiplied by the factor $v^{2/5}$ to separate the *glory* pattern from the behavior of the average component of the cross section. It has been also demonstrated that $Q(v)$ measured under the present experimental conditions depends, especially at low and intermediate v, essentially on elastic scattering.[33]

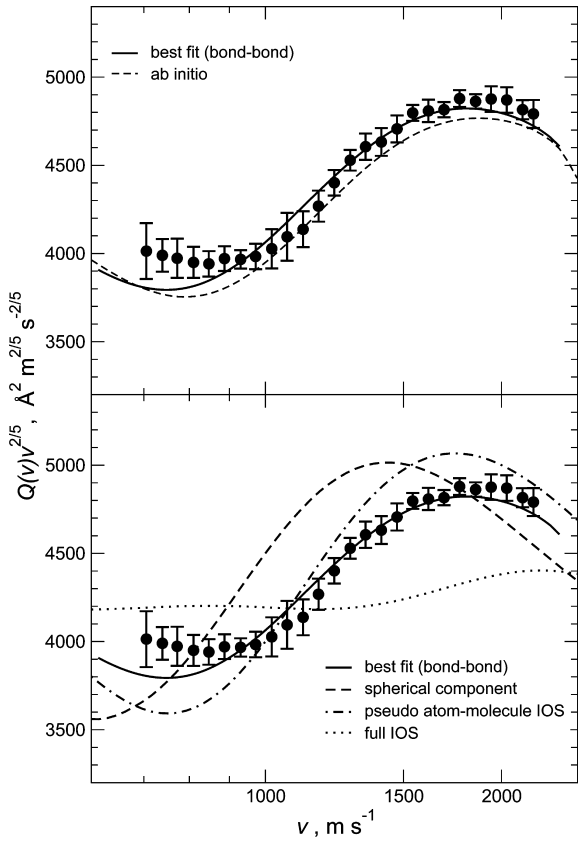

Figure 3. Total integral cross sections for scattering of nearly effusive MB of D_2 by C_2H_2 target as a function of the MB velocity v. Solid and dashed lines refer to final calculations performed with bond−bond and ab initio[35] PESs, respectively. Other lines refer to calculations performed with various dynamical models exploiting the bond−bond PES.

As in previous measurements with acetylene scattered by rare gases,[11−13] we expect $Q(v)$ to be determined by different collisional regimes, which selectively depend on the ratio between the rotational time t_{av} required to induce an average of the interaction between limiting configurations of the complex, directly related to the molecular monomer rotational period, and the average collision time, t_{coll}, which varies with the MB velocity.[36]

A more careful and extensive evaluation of this ratio than what was done in the past[11−13] becomes here necessary since we are dealing with molecule−molecule collisions with the target C_2H_2 in the scattering chamber at 90 K. To this purpose it is relevant to note that both projectile (D_2) and the target (C_2H_2) molecule exhibit a distribution of the rotational level j that change with the used experimental conditions. Table 3 reports the most probable j values together with the corresponding rotational period τ_j and the average collision time t_{coll}, evaluated at the highest, the lowest and at the intermediate MB velocities investigated. An analysis of the data reported in Table 3 suggests that C_2H_2 target can be considered rotationally sudden under all the collisional conditions. At variance with C_2H_2, the behavior of D_2 projectiles depends on both the rotational state and velocity. Specifically, molecules in $j = 0$ are obviously always rotationally sudden, but this behavior is restricted to intermediate and high velocities ($v \geq 1$ km/s) for molecules excited in $j = 1, 2$. Finally, D_2 projectiles have always sufficient time to induce an average of its anisotropy when colliding in higher j states.[40] Therefore, the analysis has been carried out combining IOS (infinite order sudden) cross sections, calculated in the pseudoatom (D_2)−molecule (C_2H_2) limit, with the full

TABLE 3: Relevant Characteristics of the Molecules in the MB and Scattering Chamber under the Present Experimental Conditions

D_2 Projectile		
nozzle temp (K)	ortho	para
	most populated j levels	
300	$j = 2, 4$	$j = 1, 3$
90	$j = 2, 0$	$j = 1$
	rotational period τ_j	
	$\tau_4 = 2 \times 10^{-13}$ s	$\tau_3 = 3 \times 10^{-13}$ s
	$\tau_2 = 4 \times 10^{-13}$ s	$\tau_1 = 8 \times 10^{-13}$ s
	$\tau_0 = \infty$	

C_2H_2 Target		
scattering chamber temp (K)	ortho	para
	most populated j levels	
90	$j = 3, 5$	$j = 4, 6$
	rotational period τ_j	
	$\tau_5 = 3 \times 10^{-12}$ s	$\tau_6 = 2 \times 10^{-12}$ s
	$\tau_3 = 4 \times 10^{-12}$ s	$\tau_4 = 3 \times 10^{-12}$ s

Average Collision Time		
lowest velocity	intermediate velocity	highest velocity
$t_{coll} = 1 \times 10^{-12}$ s	$t_{coll} = 6 \times 10^{-13}$ s	$t_{coll} = 3 \times 10^{-13}$ s

IOS cross sections obtained taking into account the full anisotropy of the PES. The relative weights of the two contributions are 2/3 and 1/3, respectively: they have been estimated by an analysis of the rotational state distributions and taking into account that at low collision velocities the increase of t_{coll} is balanced by a higher τ (in average) due to the use of cold MB. For this reason the weights of the two contributions have been assumed to be constant at all collision velocities.

Scattering cross sections have been calculated in the center of mass systems, by exploiting an efficient semiclassical technique.[41] The calculated cross sections have been then convoluted in the laboratory frame and compared in Figure 3 with the experimental data.

IV. Pressure Broadening Coefficient Calculations

The MOLSCAT quantum dynamical code[42] allows the determination of both binary diffusion S-matrix elements and collisional broadening cross sections.[43,44] The latter are therefore obtained within the framework of the impact approximation.[45,46]

The way of performing the close-coupling calculations with the MOLSCAT package is very similar to that previously used by one of us to test the ab initio PES for this system,[35,47] and thus we only mention the main change. In the present study, the coupled equations are solved by using the diabatic modified log-derivative propagator from a minimum distance of 3 Å to an intermediate one of 12 Å and with the Airy propagator up to a maximum intermolecular distance $R = 22$ Å.

The quantity which can be compared to experimental data is the pressure broadening coefficient, the collisional hwhm, which is given by

$$\gamma(j_a) = \frac{n_{H_2}\bar{v}}{2\pi c}\sigma(j_a, T) \tag{9}$$

where n_{H_2} is the density of natural hydrogen and $\bar{v} = (8k_BT/\pi\mu)^{1/2}$ is the mean relative speed at temperature T, with $\mu = 1.87$ u being the reduced mass of the colliding pair.

The PB coefficient is normally obtained through a Maxwell−Boltzmann thermal average over the relative kinetic energies of kinetic energy dependent PB cross sections

$$\sigma(j_a, T) = \frac{1}{(k_BT)^2}\int \sigma(j_a, E_{kin})E_{kin}\exp(-E_{kin}/k_BT)\,dE_{kin} \tag{10}$$

Since hydrogen molecules are composed of two assumed noninterconverting species, the thermally averaged pressure broadening cross section of an acetylene j_a line is

$$\sigma(j_a, T) = \frac{1}{4}\sigma_{pH_2}(j_a, T) + \frac{3}{4}\sigma_{oH_2}(j_a, T) \tag{11}$$

where pH_2 stands for para-hydrogen while oH_2 stands for ortho-hydrogen. For instance, the para contribution to the above total cross section is given by

$$\sigma_{pH_2}(j_a, T) = \sum_{j_b\text{even}} \rho_{j_b}\sigma(j_a, j_b, T) \tag{12}$$

where ρ_{j_b} is the H_2 (unit) normalized rotational populations for the H_2 species at a given temperature T.

The generalized[42−46] PB cross sections which enter in the right-hand side of eq 12, in the rigid approximation, are a sum of ordinary two-states to two-states rotational inelastic rate coefficients for the case of Raman isotropic Q lines, while for IR lines they comprise an additional contribution due to elastic collisions.[43,45,46]

In this study we have skipped the thermal average integration because we are mainly interested in the comparison between semiempirical and ab initio PESs; therefore we have simply perfomed the calculations at kinetic energies $\bar{E}_{kin}/hc = 126.5$, 153, and 261 cm^{-1} associated with the mean relative speed at temperatures $T = 143$, 173, and 295 K. This approximation should have less importance as the temperature increases.

V. Optimization of the PES and Comparisons with Experimental Results

The parameters of the bond−bond PES have been optimized in order to best fit the experimental ICS and at the same time to reproduce as good as possible the PB coefficients. In general, the ICS data are more sensitive to the well of the PES and its long range part while the PB cross sections are more sensitive to the short range. Therefore these two types of experimental data are complementary. It should be noted that the parameters allowed to vary in the fit are very few and, moreover, dependencies exist between some of them (see Appendix A of ref 23). The final best fit values differ from the predicted ones (see Table 1 and Appendix A of ref 23) only by few percent.

The final comparison among calculated quantities and experimental data (see below) shows a very good agreement. This is not always obvious in a multiproperty analysis, and therefore it is simultaneously a demonstration of the good predicting power of the correlation formulas (see Appendix A of ref 23) and a satisfactory test of the flexibility of the analytical parametrization employed for the bond−bond PES.

It is interesting to assess the sensitivity of the MB scattering data to the features of the PESs. Figure 3 also shows the results of each ICS calculation, carried out with the bond−bond PES within the various dynamical regimes discussed above and also

TABLE 4: Comparison between Calculated Pressure Broadening Cross Sections (in Å^2) for Isotropic Raman Q Lines: First Line with the Present Bond−Bond PES, Second Line with the Ab Initio PES (Calculated Values at the Single Kinetic Energy $\bar{E}_{kin}/hc = 126.5$ cm^{-1}) and Third Line Thermally Averaged Values Obtained with the Ab Initio PES[49] [a]

line	σ_{pH_2}	σ_{oH_2}	σ	γ (calcd)	γ (exptl)
Q2	36.63	43.66	41.90	145.25	139.6 ± 28
	30.64	39.87	37.57	130.24	
	30.08	38.93	36.72	127.25	
Q4	39.28	46.05	44.36	153.77	144.0 ± 8
	33.46	42.39	40.15	139.20	
	32.02	40.51	38.39	132.99	
Q6	40.29	47.45	45.66	158.29	149.0 ± 11
	34.30	43.35	41.09	142.35	
	32.90	41.30	39.20	135.83	
Q7	40.43	47.81	45.96	159.34	141.1 ± 8
	34.70	43.72	41.46	143.74	
	33.24	41.10	39.14	135.63	
Q10	40.37	47.21	45.50	157.73	142.2 ± 17
	34.34	43.15	40.94	141.94	
	33.70	41.45	39.51	136.91	

[a] Resulting pressure broadening coefficients (γ in 10^{-3} cm^{-1}/atm) are compared with measured values at 143 K.[35]

exploiting the spherical average interaction (i.e., assuming that both molecules have sufficient time for the interaction anisotropy to be completely washed out). The figure shows that the frequency of the glory pattern is determined by the depth and location of the potential well of the spherically averaged interaction and the absolute scale of $Q(v)$ depends on its long-range attraction (see also note in ref 40). Therefore, the present scattering data allow a characterization of strength and range of the spherical component within 7% and 3%, respectively. Moreover, the interaction anisotropy induces a shift of the glory extrema position and a partial quenching of the glory amplitude.[48] Since the ICS data are not very sensitive to details of the short-range interaction anisotropy, these effects are similar for both the ab initio and bond−bond PESs.

For the ab initio PESs the overall agreement with the experimental ICS data is also satisfactory considering that no-scaling parameters have been introduced in the ab initio calculations. More specifically, the position of the calculated glory extrema is slightly shifted at higher collision velocity with respect to the experimental one. This is due to the slightly larger well area of the spherical interaction component of the ab initio potential. The ab initio PES provides an absolute value of the ICS slightly lower with respect to the bond−bond PES because the long-range interaction is slightly less attractive.

The analysis of PB coefficients includes experimental data as well as previous results obtained exploiting the ab initio PES.[35] Table 4 and Figure 4 compare calculated and measured results for isotropic Raman lines at 143 K.[35] While the PB coefficients obtained at $\bar{E}_{kin}$ with the present bond−bond PES are systematically larger than the experimental data (up to 13%), the values obtained from the ab initio PES are smaller than the experimental data (up to −6.7%). Comparisons between line 2 and line 3 of Table 4 allow the prediction that the correct thermally averaged values using the bond−bond PES should be lower by about 4%. Using the ab initio PES, the thermally averaged values obtained are indeed smaller than the values obtained without performing this average. This is due to the variation of the pressure broadening cross sections with the kinetic energy (see Figure 3 of ref 35) and the shape of the Maxwell−Boltzmann kinetic energy distribution. This is even more true for the ortho-contribution, which has the largest weight to the total PB cross section. The present results are therefore quite good considering the large experimental uncertainties.

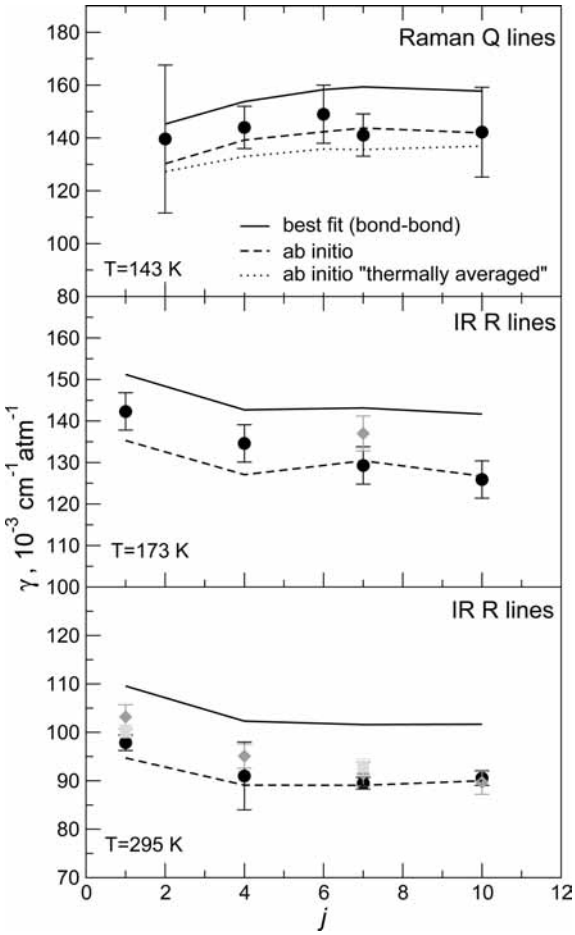

Figure 4. Calculated PB coefficients obtained by using present bond−bond (solid line) and ab initio[35] (dashed line) PESs. Upper panel: Isotropic Raman Q lines. Thermally averaged results (dotted line) obtained with the ab initio PES are also added. Experimental results (full circles) at 143 K are from ref 35. Intermediate panel: IR R lines. Experimental results (full circles and full diamond) at 173 K are from refs 51 and 50. Lower panel: IR R lines. Experimental results (full circles, full squares, and full diamonds) at 295 K are from refs 50, 52, and 53.

Comparisons between three sets of data, i.e., our present calculations, previous calculations,[47] and experimental data,[50−53] for acetylene IR lines in baths of H_2 at 173 and 295 K are gathered in Table 5 and also shown in Figure 4. Here too we observe that the present calculated values are larger than both previous calculations and experimental data. However, they are in reasonable agreement (from 6 to 12%) with the experimental values.

The relative difference between both set of calculations (compare lines 1 and 2 of Tables 4 and 5) is more pronounced for the para contribution (essentially $j_b = 0$) than for the ortho contribution to the total PB cross sections. This may be due partly to the fact that for $j_b = 0$ the dynamic is more sensitive to the isotropic part of the PES.[35] The area of the isotropic component of the bond−bond PES is smaller than the corresponding area of the ab initio PES (see Figure 2); the anisotropic component is however only slightly smaller than the corresponding component of the ab initio PES, hence giving rise to larger cross sections. However, the dynamical calculations

TABLE 5: Comparison between Calculated Pressure Broadening Cross Sections (in Å^2) for IR R Lines: First Line with the Present Bond−Bond PES, Second Line with the Ab Initio PES (Unthermally Averaged Values of Reference 47)[a]

$\bar{E}_{kin}$/cm^{-1}	line	σ_{pH_2}	σ_{oH_2}	σ	γ (calcd)	γ (exptl)
153	R1	43.52	49.45	47.97	151.20	142.3 ± 4.5[b]
		38.01	44.57	42.93	135.30	
153	R4	40.72	46.79	45.27	142.69	134.6 ± 4.5[b]
		34.27	42.33	40.32	127.08	
153	R7	40.68	46.99	45.41	143.13	129.3 ± 4.5[b]
		34.49	43.67	41.38	130.41	137 ± 4.2[c]
153	R10	40.41	46.46	44.95	141.67	125.9 ± 4.5[b]
		34.13	42.23	40.20	126.72	
261	R1	43.21	46.12	45.39	109.56	97.85 ± 1.6[d]
		35.76	40.40	39.24	94.71	103 ± 2.5[e]
						100.2 ± 1.3[c]
261	R4	40.10	42.99	42.27	102.03	91 ± 0.7[d]
		33.64	38.01	36.92	89.10	95.1 ± 2.5[e]
261	R7	39.80	42.85	42.09	101.59	89.5 ± 1.2[d]
		33.74	37.95	36.90	89.06	91.4 ± 2.5[e]
						92.8 ± 1.7[c]
261	R10	39.79	42.89	42.12	101.66	90.55 ± 1.5[d]
		33.83	38.44	37.29	90.00	89.7 ± 2.5[e]

[a] Resulting pressure broadening coefficients (γ in 10^{-3} cm^{-1}/atm) are compared with measured values at 173 and 295 K. [b] From ref 51. [c] From ref 50. [d] From ref 52. [e] From ref 53.

performed here do not sample a large part of the PES. Indeed, using a semiclassical argument one can estimate an effective scaling length b giving the range probed by the PB cross sections through: $\sigma = \pi b^2$. Even at the lowest kinetic energy employed (126.5 cm^{-1}) b is not greater than about 4 Å. More importantly, the calculated PB cross sections using the bond−bond PES are greater than those predicted by the ab initio PES because the former is more anisotropic at short range.

In addition, we remark that the differences between the two sets of calculations are more important for the highest j values than for the lower ones. Generally speaking, low j values are more sensitive than high j values to the long-range part of a PES, which in turn are more sensitive to the repulsive part of a PES (see refs 35 and 47 and references therein). Since the present bond−bond PES is more repulsive than the ab initio one, the PB cross section for the highest j values are larger than those previously published.[35,47]

VI. Summary and Conclusions

This paper demonstrates the importance of coupling theoretical and experimental results to obtain a formulation of the PES suitable to describe accurately both stable and less stable configurations of interacting systems. The bond−bond methodology provides a relatively simple analytical formulation of the PES which involves a limited number of potential parameters, having each one a physical meaning being related to specific properties of the interacting partners. Moreover, zero-order parameters can be anticipated by general correlation formulas and they can be fine-tuned analyzing experimental data and/or by comparison with results of ab initio calculations.

The bond−bond PES is faster to compute[56] than the ab initio PES and its mathematical expression may be useful to carry out extensive molecular dynamic simulations especially those based on classical mechanics for which analytical derivatives are needed. These properties allow the parameters of this PES to be further refined using other experimental data.

The methodology has been here tested on the acetylene−hydrogen system and is promising to be further extended to molecule/radical-molecule systems of increasing complexity for which ab initio calculations or experimental data are very hard to be obtained. As an example, this could be important to predict and assess the role of long-range forces on the molecular reactivity at low temperatures, which can selectively emerge in various environments, as for instance in interstellar clouds.[57]

The PES presented in this work is available, as FORTRAN subroutines, upon request to the corresponding author.

Acknowledgment. The work in Perugia has been supported by the Italian Ministero della Universitá e Ricerca (MIUR) through the PRIN programme. M.B. was supported by the "JAEdoc" programme of Consejo Superior de Investigaciones Científicas and by the Ministerio de Educación y Ciencia (Spain, Grant CTQ 2007-62898-BQU). The French team thanks the CNRS (Centre National de la Recherche Scientifique) for its financial support.

References and Notes

(1) Encrenaz, Th.; Drossart, P.; Feuchtgruber, H.; Lellouch, E.; Bezard, B.; Fouchet, T.; Atreya, S. K. *Planet. Space Sci.* **1999**, *47*, 1225. Sada, P. V.; Bjoraker, G. L.; Jennings, D. E.; Romani, P. N.; McCabe, G. H. *Icarus* **2005**, *173*, 499. (b) Lorenz, R. *J. Phys. IV* **2002**, *12*, 281.

(2) Warnatz, R. W. D. J.; Maas, U. *Combustion*; Springer-Verlag: Berlin, Heidelberg, and New York, 2001.

(3) Lamprecht, A.; Atakan, B.; Kohse-Hoinghaus, K. *Combust. Flame* **2000**, *122*, 483.

(4) Buldyreva, J.; Bonamy, J.; Weikl, M.; Beyrau, F.; Seeger, T.; Leipertz, A.; Vestin, F.; Afzelius, M.; Bood, J.; Bengtsson, P.-E. *J. Raman Spectrosc.* **2006**, *37*, 647.

(5) Robertson, J. *Mater. Sci.Eng., R* **2002**, *37*, 129.

(6) Richter, H.; Howard, J. B. *Prog. Combust. Sci.* **2000**, *26*, 565.

(7) Cojocaru, C. S.; Senger, A.; Le Normand, F. *J. Nanosci. Nanotechnol.* **2006**, *6*, 1331.

(8) *Intermolecular Forces, Adv. Chem. Phys.*; Hirschfelder, J. O., Ed.; Advances in Chemical Physics, Vol. 12; Wiley: New York, 1967.

(9) Maitland, G. C.; Rigby, M.; Smith, E. B.; Wakeham, W. A. *Intermolecular Forces*; Clarendon Press: Oxford, 1987.

(10) Stone, A. J. *The Theory of Intermolecular Forces*; Clarendon Press: Oxford, 1996.

(11) Cappelletti, D.; Bartolomei, M.; Sabido, M.; Pirani, F.; Blanquet, G.; Walrand, J.; Bouanich, J.-P.; Thibault, F. *J. Phys. Chem.* **2005**, *109*, 8471.

(12) Cappelletti, D.; Bartolomei, M.; Carmona-Novillo, E.; Pirani, F.; Blanquet, G.; Thibault, F. *J. Chem. Phys.* **2007**, *126*, 064311.

(13) Thibault, F.; Cappelletti, D.; Pirani, F.; Blanquet, G.; Bartolomei, M. *Eur. Phys. J. D* **2007**, *44*, 337.

(14) Herbst, E. *Annu. Rev. Phys. Chem.* **1995**, *46*, 27.

(15) Ahlrichs, R.; Penco, R.; Scoles, G. *Chem. Phys.* **1977**, *19*, 119.

(16) Tang, K. T.; Toennies, J. P. *J. Chem. Phys.* **1977**, *66*, 1496.

(17) Douketis, C.; Scoles, G.; Marchetti, S.; Zen, M.; Thakkar, A. J. *J. Chem. Phys.* **1982**, *76*, 3057.

(18) Tang, K. T.; Toennies, J. P. *J. Chem. Phys.* **1984**, *80*, 3726.

(19) Pirani, F.; Liuti, G. *Chem. Phys. Lett.* **1985**, *122*, 245.

(20) Cambi, R.; Cappelletti, D.; Pirani, F.; Liuti, G. *J. Chem. Phys.* **1991**, *95*, 1852.

(21) Cappelletti, D.; Liuti, G.; Pirani, F. *Chem. Phys. Lett.* **1991**, *183*, 297.

(22) Halgren, T. A. *J. Am. Chem. Soc.* **1992**, *114*, 7827.

(23) Cappelletti, D.; Pirani, F.; Bussery-Honvault, B.; Gomez, L.; Bartolomei, M. *Phys. Chem. Chem. Phys.* **2008**, *10*, 4281.

(24) Bartolomei, M.; Cappelletti, D.; de Petris, G.; Moix Teixidor, M.; Pirani, F.; Rosi, M.; Vecchiocattivi, F. *Phys. Chem. Chem. Phys.* **2008**, *10*, 5993.

(25) Pirani, F.; Cappelletti, D.; Liuti, G. *Chem. Phys. Lett.* **2001**, *350*, 286.

(26) Pirani, F.; Albertí, M.; Castro, A.; Moix Teixidor, M.; Cappelletti, D. *Chem. Phys. Lett.* **2004**, *37*, 394.

(27) Pirani, F.; Brizi, S.; Roncaratti, L.; Casavecchia, P.; Cappelletti, D.; Vecchiocattivi, F. *Phys. Chem. Chem. Phys.* **2008**, *10*, 5489. perspective article.

(28) Pack, R. T. *Chem. Phys. Lett.* **1978**, *55*, 197.

(29) Candori, R.; Pirani, F.; Vecchiocattivi, F. *Chem. Phys. Lett.* **1983**, *102*, 412.

(30) Beneventi, L.; Casavecchia, P.; Volpi, G. G. *J. Chem. Phys.* **1986**, *85*, 7011.

(31) Beneventi, L.; Casavecchia, P.; Pirani, F.; Vecchiocattivi, F.; Volpi, G. G.; Brocks, G.; van der Avoird, A.; Heijmen, B.; Reuss, J. *J. Chem. Phys.* **1991**, *95*, 195.

(32) Karimi-Jafari, M. H.; Ashouri, M.; Yeganeh-Jabri, A. *Phys. Chem. Chem. Phys.*, in press.

(33) Aquilanti, V.; Ascenzi, D.; Bartolomei, M.; Cappelletti, D.; Cavalli, S.; de Castro Vítores, M.; Pirani, F. *J. Am. Chem. Soc.* **1999**, *121*, 10794.

(34) Gomez, L.; Bussery-Honvault, B.; Cauchy, T.; Bartolomei, M.; Cappelletti, D.; Pirani, F. *Chem. Phys. Lett.* **2007**, *445*, 99.

(35) Thibault, F.; Corretja, B.; Viel, A.; Bermejo, D.; Martínez, R. Z.; Bussery-Honvault, B. *Phys. Chem. Chem. Phys.* **2008**, *10*, 5419.

(36) Cappelletti, D.; Bartolomei, M.; Pirani, F.; Aquilanti, V. *J. Phys. Chem. A* **2002**, *106*, 10764.

(37) Aquilanti, V.; Cappelletti, D.; Pirani, F.; Roncaratti, L. *Int. J. Mass Spectrom.* **2009**, *280*, 72.

(38) Nenner, T.; Tien, H.; Fenn, J. B. *J. Chem. Phys.* **1975**, *63*, 5439.

(39) Pirani, F.; Vecchiocattivi, F. *J. Chem. Phys.* **1977**, *66*, 372.

(40) Note that the average component of $Q(v)$ is determined by the elastic scattering associated to the long range attraction component of the isotropic part of the intermolecular interaction, while the glory pattern, arising from collisional events at intermediated impact parameters, depends on range and strength of the interaction in proximity of the well. In particular, the amplitude of the glory effect is affected by the interaction anisotropy near the equilibrium distance and only partially by inelastic events which are of some relevance mostly for molecules colliding with $j = 0$ (see for instance: Aquilanti, V.; Beneventi, L.; Grossi, G.; Vecchiocattivi, F. *J. Chem. Phys.* **1988**, *89*, 751.

(41) Pirani, F.; Vecchiocattivi, F. *Mol. Phys.* **1982**, *45*, 1003.

(42) Hutson, J. M.; Green, S. *MOLSCAT version 14, Collaborative Computational Project 6 of the UK Science and Engineering Research Council*; Daresbury Laboratory: U.K., 1995.

(43) Green, S. *Chem. Phys. Lett.* **1977**, *47*, 119.

(44) Shafer, R.; Gordon, R. G. *J. Chem. Phys.* **1973**, *58*, 5422.

(45) Ben-Reuven, A. *Phys. Rev.* **1966**, *141*, 34.

(46) Ben-Reuven, A. *Phys. Rev.* **1966**, *145*, 7.

(47) Thibault, F.; Fuller, E. P.; Grabow, K. A.; Hardwick, J. L.; Marcus, C. I.; Marston, D.; Robertson, L. A.; Senning, E. N.; Stoffel, M. C.; Wiser, R. S. *J. Mol. Spectrosc.* **2009**, *256*, 17.

(48) Previous total differential cross section measurements(Yang, M.; Watts, R. O. *J. Chem. Phys.* **1994**, *100*, 3582.) were performed at a collision energy higher than those probed in the present experiment. The observation of few quenched diffraction oscillations provided only semiquantitative information on range and strength of the interaction.

(49) There is a mistake in Table 3 of ref 35. The values presented are not the thermally averaged values but calculated at the kinetic energy of 126.5 cm^{-1}.

(50) Varanasi, P. *J. Quant. Spectrosc. Radiat. Transfer* **1992**, *47*, 263.

(51) Bouanich, J. P.; Walrand, J.; Blanquet, G. *J. Mol. Spectrosc.* **2002**, *216*, 266.

(52) Arteaga, S. W.; Bejger, C. M.; Gerecke, J. L.; Hardwick, J. L.; Martin, Z. T.; Mayo, J.; McIlhattan, E. A.; Moreau, J. M. F.; Pilkenton, M. J.; Polston, M. J.; Robertson, B. T.; Wolf, E. N. *J. Mol. Spectrosc.* **2007**, *243*, 253.

(53) Lambot, D.; Blanquet, G.; Walrand, J.; Bouanich, J. P. *J. Mol. Spectrosc.* **1991**, *4150*, 164.

(54) Le Roy, R. J.; Hutson, J. M. *J. Chem. Phys.* **1987**, *86*, 837.

(55) *NIST Chemistry WebBook, NIST Standard Reference Database Number 69*; Linstrom, P. J., Mallard, W. G., Eds.; 2005; http://WebBook.nist.gov.

(56) As an example the CPU time for 10000 geometries on an Intel Xeon Dual Core is 0.044 s with the present PES and 5.78 s with the ab initio PES which is built on a four-dimensional grid and therefore calls bicubic splines routines. We note however that for the specific case of PB calculations with the MOLSCAT code there is no CPU time difference because both PESs are beforehand projected over bispherical harmonics and the (tabulated) radial coefficients stored on disk files for further processing. The CPU time required to rebuild the PES from its development over bispherical harmonics is 0.45 s.

(57) Sims, I. R.; Queffelec, J. L.; Travers, D.; Rowe, B. R.; Herbert, L. B.; Karthauser, J.; Smith, I. W. M. *Chem. Phys. Lett.* **1993**, *211*, 461.

JP905055N